A numerical tool for thermo-mechanical analysis of multilayer stepped structures

Paolo Emilio Bagnoli[1], Maria Girardi[*2], Cristina Padovani[2] and Giuseppe Pasquinelli[2]

[1]*Department of Information Engineering, University of Pisa, Via G. Caruso 16 56122, Pisa, Italy*
[2]*Institute of Information Science and Technologies "A. Faedo", National Research Council of Italy ISTI-CNR, Via G. Moruzzi 1, 56124, Pisa, Italy*

Abstract. An integrated simulation tool for multilayer stepped pyramidal structures is presented. The tool, based on a semi-analytical mathematical strategy, is able to calculate the temperature distributions and thermal stresses at the interfaces between the layers of such structures. The core of the thermal solver is the analytical simulator for power electronic devices, DJOSER, which has been supplemented with a mechanical solver based on the finite-element method. To this end, a new ele-ment is proposed whose geometry is defined by its mean surface and thickness, just as in a plate. The resulting mechanical model is fully three-dimensional, in the sense that the deformability in the direction orthogonal to the mean surface is taken into account. The dedicated finite element code developed for solving the equilibrium problem of structures made up of two or more superimposed plates subjected to thermal loads is applied to some two-layer samples made of silicon and copper. Comparisons performed with the results of standard finite element analyses using a large number of brick elements reveal the soundness of the strategy employed and the accuracy of the tool developed.

Keywords: multilayer structures, thermal stresses, finite element method, power electronic devices

1. Introduction

Power electronic devices are composed of structures made up of layers with different geometrical and thermo-mechanical properties. These structures are subjected to high thermal loads, which give rise to stress distributions that can damage the adhesive films between the layers and lead to debonding. The problem of the thermal analysis of such structures has been addressed in (Bagnoli *et al.* 2007a, Bagnoli *et al.* 2007b, Montesi *et al.* 2004), where DJOSER, a tool for computing the steady-state temperature mapping of multilayer assembly structures for power electronics, is described. The simplicity and high degree of standardization of power assemblies, which in most cases can be modeled as multilayer, stepped pyramidal structures with homogeneous layers and rectangular geometries, enable fruitful application of DJOSER, which is a time saving, user-friendly code based on an analytical approach.

∗Corresponding author, Ph.D., E-mail: maria.girardi@isti.cnr.it

From a thermo-mechanical point of view, software tools that enable calculating both the tangential and normal stresses, and thereby assessing the quality of adhesion and locating eventual critical zones, are of fundamental importance. The crucial role of numerical modeling is testified to by a large number of recent publications focusing on obtaining approximations and estimates of the interlaminar thermal stresses in multilayer structures, (Hsueh *et al.* 2006, Crosby and Ghoniem 2011, Wu 2004, Saidi *et al.* 2013, Simhonian and Sanoyan 2009, Xie and Sitaraman 2000), as well as on numerical procedures for thermo-mechanical analysis of composite and sandwich plates, (Zhen and Chen 2007, Carrera 2004, De Borst and Sadowski 2008, Gherlone and Di Sciuva 2007, Grigolyuk and Tolkachev 1980, Grigolyuk *et al.* 1994, Grigolyuk *et al.* 1995, Lo *et al.* 2011, Roaldo 2006). A method for reducing the bending stresses in the low strength materials of the multilayer composite structures used in electronic packaging subjected to temperature changes is proposed in Suhir and Weld (1998). The method is based on the application of a 'surrogate' layer of a high expansion (contraction) and/or high modulus material aimed at flattening the structure. A stress analysis model for the evaluation of stresses, strains and displacements induced by thermal variations in the 'piecewise continuous' adhesive layer between two identical non-deformable adherends is presented in Suhir (2000). Similarly, Suhir (2011) develops simple, easy-to-use, physically meaningful predictive analytical models for evaluating the interfacial shearing and normal stresses in the bonding material of a die-carrier assembly.

An analytical approach has been also followed in Bagnoli *et al.* (2008), Bagnoli *et al.* (2009), Bagnoli *et al.* (2011), where the authors consider a one-dimensional problem for both geometry and thermal loads, with only one interface, in which the presence of contact thermal resistance causes an abrupt change in the temperature field. The expressions for the stresses deduced analytically within the framework of the Love-Kirchhoff theory, published in Timoshenko and Woinowsky-Krieger (1959) have been introduced into three-dimensional constitutive equations, expressed as functions of the derivatives of displacements. This enables the strain-displacement equations to be integrated, thus yielding the expressions for the displacements along the thickness. A finite difference algorithm is implemented to solve the system of integro-differential equations governing the equilibrium of the layers with the proper boundary conditions and the contact conditions guaranteeing adherence between the different layers.

When generalized to three-dimensional structures, this approach would lead to a very complex system of equations, and using finite difference methods to solve this system might not be advantageous in terms of implementation and computational costs.

The goal of the current paper is to present and test a numerical code, which like the tool proposed in (Bagnoli *et al.* 2011), for one-dimensional problems, is called THESIS. It is based on the finite element method Zienkiewicz and Taylor (1989) for multilayer pyramidal structures and enables predicting thermally induced stresses at their interfaces. The code is aimed at managing structures largely employed in power electronics, with simple geometries and subjected to thermal loads; no mechanical loads are taken into account.

Although herein we limit ourselves to applying the numerical method to the analysis of two-layer three-dimensional structures (Fig. 1(a) and (b)), it can be easily extended to multilayer structures. We present a new element whose geometry is defined by its mean surface and thickness, as in plates, and whose mechanical behavior is modeled as fully three-dimensional, in the sense that the deformability in the direction orthogonal to the mean surface is taken into account.

The element has been implemented in the finite element code THESIS, which when coupled with DJOSER, can be applied to solving the equilibrium problem of structures made up of two or

more superimposed linear elastic layers subjected to thermal loads.

As in previous works by Bagnoli *et al.* (2008), Bagnoli *et al.* (2009), Bagnoli *et al.* (2011), the temperatures calculated by DJOSER are used as input data for the mechanical solver. The output variables are the normal stresses Q_i^-, Q_i^+ and the shear stresses P_i^-, P_i^+ respectively on the lower and upper surfaces of the *i*-th layer (Fig. 1(c)).

The code is applied to some two-layer samples made of silicon and copper, with thicknesses h_2 and h_1, respectively, as the number of elements is varied. With the aim of assessing the accuracy of the numerical, a comparison with standard finite element analyses using a large number of brick elements is then performed.

2. The numerical procedure

2.1 The thermal solver

As pointed out in Section 1, the temperature fields for the steady-state case are calculated by applying the DJOSER analytical thermal solver, whose mathematical background is thoroughly described in Bagnoli *et al.* (2007a), Bagnoli *et al.* (2007b), Montesi *et al.* (2004).

From the practical point of view, the calculation procedure consists of two steps. First, regular grids composed of rectangular cells are defined on the top and bottom surfaces of each layer, and the system of integral equations delivering the temperature T and heat flux q is transformed into an algebraic system. Numerical solution of the system yields the values $(T_j^{(i)}, q_j^{(i)})$, where j indicates the cell number and i the layer number.

In the second step, more accurate temperature maps can be calculated with any spatial resolution using the same numerical equation valid for the top surface of each layer and the set of previously calculated temperature and flux values.

The performance of the mechanical solver described in Subsection 2.2 improves if the temperatures are assigned not only on the top and bottom surface of each layer, but also on three planes within the bulk of the layer, as shown in Fig. 1(d). Therefore, a more complete equation for temperature calculation is needed here to include the dependence on the depth within the layer.

For x, y and z the Cartesian coordinates, L_x, L_y and L_z the dimensions of a layer constituting the step pyramidal structure and k the thermal conductivity, the analytical expression for temperature T is, as shown in Bagnoli *et al.* (2007a)

$$T(x, y, z) = \frac{L_z}{k} \sum_{n=1}^{\infty} \sum_{m=1}^{\infty} \frac{X(\beta_n x) \cdot Y(\mu_m y)}{N(\beta_n) \cdot N(\mu_m)} \times$$

$$\frac{\upsilon_{n,m} L_z \cosh\left[\upsilon_{n,m}(L_z - z)\right] + B_i(5)\sinh\left[\upsilon_{n,m}(L_z - z)\right]}{L_x L_y S(n,m)} \int_0^{L_x} \int_0^{L_y} f(x', y') X(\beta_n x') Y(\mu_m y') \, dx' dy' +$$

$$\frac{\upsilon_{n,m} L_z \cosh(\upsilon_{n,m} z) + B_i(0)\sinh(\upsilon_{n,m} z)}{L_x L_y S(n,m)} \int_0^{L_x} \int_0^{L_y} g(x', y') X(\beta_n x') Y(\mu_m y') \, dx' dy' \qquad (2.1)$$

where $\upsilon^2_{n,m} = \beta_n^2 + \mu_n^2$ and the eigenfunctions X and Y, which depend on the eigenvalues β_n and μ_n

and on the Biot numbers $B_i(j)$ if lateral convection is present, have the following expressions

$$X(\beta_n \mathrm{x}) = \beta_n L_\mathrm{x} \cos(\beta_n \mathrm{x}) \;+\; B_i(1)\sin(\beta_n \mathrm{x}) \tag{2.2}$$

$$Y(\mu_m \mathrm{y}) \;= \mu_m L_\mathrm{y} \cos(\mu_m \mathrm{y}) \;+\; B_i(3)\sin(\mu_m \mathrm{y}) \tag{2.3}$$

$N(\beta_n)$ and $N(\mu_n)$ are the norms of the eigenfunctions X and Y, while $S(n,m)$ is independent of the coordinates. The functions f and g are the top incoming heat flux and the bottom temperature distributions. The coordinates x, y, z within the single layer indicate the point at which the temperature is calculated, while the integration variables x', y' over the top surface, after discretization of the equation, represent the centers of the cells of the top and bottom rectangular grids, respectively. Eq. (2.1) allows for calculating the temperature T within the plate thickness for different values of z. By way of example, Fig. 2 shows the behavior of temperatures in the silicon and copper layers calculated at the five values of z shown in Fig. 1(d) for sample "S" described in the next Section. The plots correspond to the cross-section where the maximum values of temperatures are reached.

2.2 The mechanical solver

Herein we describe the numerical method introduced in Bagnoli et al. (2010) for solving the equilibrium problem of structures, often employed in power electronics, made up of superimposed rectangular linear elastic layers with different geometric and thermo-mechanical properties subjected to high thermal loads (Fig. 1). The thermo-mechanical solver presented here is based on the finite element method described in Zienkiewicz and Taylor (1989) and is aimed at calculating
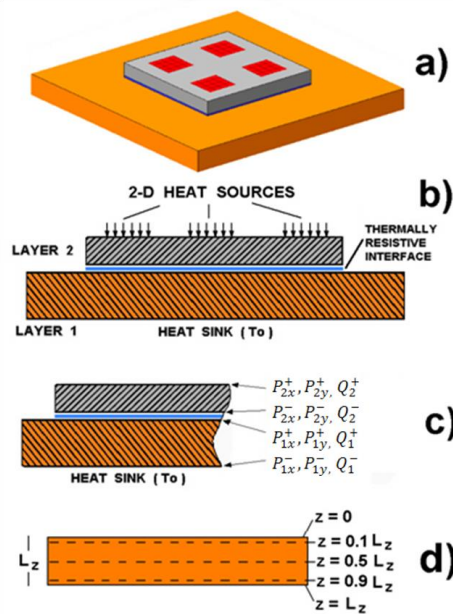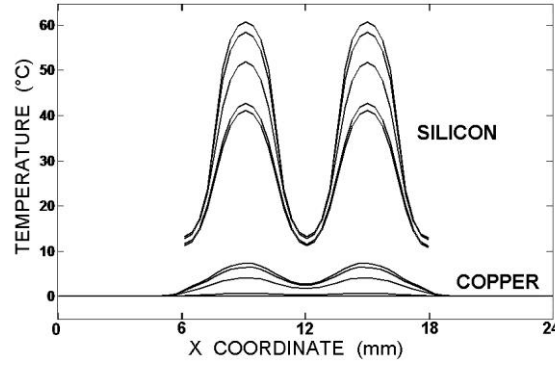

Fig. 1 The multilayer pyramidal structure

Fig. 2 Cross-section plots of the temperature maps produced by DJOSER and used as thermal input data for the mechanical analysis of sample "S"

the normal and shear stresses at the interface between the different layers of multilayer structures. We assume that the only loads acting on the structure are due to the thermal dilatations induced by the temperature field T, which is not continuous at the interfaces due to the presence of contact thermal resistance. The interface between two adjacent layers, whose mechanical properties are not taken into account, is modeled by imposing conditions that guarantee the adherence between the layers.

In the following we describe a new finite element that can be used to model a step pyramidal structure. We assume that the linear elastic material constituting the element is isotropic, with Young modulus E, Poisson ratio v and linear coefficient of thermal expansion α. The geometry of the element is defined by its mean surface and thickness, as in the case of plates, and its thermo-mechanical behavior is modeled as fully three-dimensional, in the sense that the deformability along the thickness is taken into account. The element is a four-node rectangle with sides parallel to the x and y coordinate axes, and the normal unit vector parallel to the z axis. The displacement field is interpolated by mean of shape functions which are linear in x and y and quadratic in z. Each node has nine degrees of freedom, i.e., three displacements each of the bottom, middle surface and top of the element. In particular, each element is characterized by the coordinates of the centroid (x_G, y_G, z_G) and the dimensions $2a$, $2b$ and h, along the x, y and z directions, respectively. The local coordinates (ξ, η, ζ) corresponding to the global coordinates (x, y, z) of any given point within the element are defined as

$$\xi = (x - x_G)/a \tag{2.4}$$

$$\eta = (y - y_G)/b \tag{2.5}$$

$$\zeta = 2(z - z_G)/h \tag{2.6}$$

The displacement vector $\mathbf{u}$ at (ξ, η, ζ) is interpolated in the following way

$$\mathbf{u}(\xi, \eta, \zeta) = \sum_{i=1}^{3}\left(\sum_{j=1}^{4} \varphi_j(\xi, \eta)\mathbf{u}_{ij} \right)\psi_i(\zeta) \tag{2.7}$$

where $\mathbf{u}_{ij}$ is the displacement vector of the *j*-th node of the bottom ($i = 1$), the top ($i = 2$) and the middle surface ($i = 3$) of the element.

The bilinear in-plane shape functions φ_i are

$$\varphi_1(\xi, \eta) = (1 - \xi)(1 - \eta)/4 \tag{2.8}$$

$$\varphi_2(\xi, \eta) = (1 + \xi)(1 - \eta)/4 \tag{2.9}$$

$$\varphi_3(\xi, \eta) = (1 + \xi)(1 + \eta)/4 \tag{2.10}$$

$$\varphi_4(\xi, \eta) = (1 - \xi)(1 + \eta)/4 \tag{2.11}$$

and the quadratic out of plane shape functions ψ_j are

$$\psi_1(\zeta) = \zeta(1 - \zeta)/2 \tag{2.12}$$

$$\psi_2(\zeta) = \zeta(1 + \zeta)/2 \tag{2.13}$$

$$\psi_3(\zeta) = (1 - \zeta)(1 + \zeta) \tag{2.14}$$

For $\nabla \mathbf{u}$, the gradient of the displacement, and $\nabla \mathbf{u}^T$, its transpose, the vector $\boldsymbol{\varepsilon}$ of the engineering components of the infinitesimal strain tensor ($\nabla \mathbf{u} + \nabla \mathbf{u}^T$)/2 at any point in the element can be easily calculated by taking into account expression (2.7). For u^x, u^y and u^z, the Cartesian components of vector $\mathbf{u}$, we have

$$\varepsilon_{xx} = \frac{1}{a} \sum_{i=1}^{3} \left(\sum_{j=1}^{4} \frac{\partial \varphi_j}{\partial \xi} u_{ij}^x \right) \psi_i \tag{2.15}$$

$$\varepsilon_{yy} = \frac{1}{b} \sum_{i=1}^{3} \left(\sum_{j=1}^{4} \frac{\partial \varphi_j}{\partial \eta} u_{ij}^y \right) \psi_i \tag{2.16}$$

$$\varepsilon_{zz} = \frac{2}{h} \sum_{i=1}^{3} \left(\sum_{j=1}^{4} \varphi_j u_{ij}^z \right) \frac{\partial \psi_i}{\partial \zeta} \tag{2.17}$$

$$\varepsilon_{xy} = \frac{1}{a} \sum_{i=1}^{3} \left(\sum_{j=1}^{4} \frac{\partial \varphi_j}{\partial \xi} u_{ij}^y \right) \psi_i + \frac{1}{b} \sum_{i=1}^{3} \left(\sum_{j=1}^{4} \frac{\partial \varphi_j}{\partial \eta} u_{ij}^x \right) \psi_i \tag{2.18}$$

$$\varepsilon_{xz} = \frac{1}{a} \sum_{i=1}^{3} \left(\sum_{j=1}^{4} \frac{\partial \varphi_j}{\partial \xi} u_{ij}^z \right) \psi_i + \frac{2}{h} \sum_{i=1}^{3} \left(\sum_{j=1}^{4} \varphi_j u_{ij}^x \right) \frac{\partial \psi_i}{\partial \zeta} \tag{2.19}$$

$$\varepsilon_{yz} = \frac{1}{b} \sum_{i=1}^{3} \left(\sum_{j=1}^{4} \frac{\partial \varphi_j}{\partial \eta} u_{ij}^z \right) \psi_i + \frac{2}{h} \sum_{i=1}^{3} \left(\sum_{j=1}^{4} \varphi_j u_{ij}^y \right) \frac{\partial \psi_i}{\partial \zeta} \tag{2.20}$$

Eqs. (2.15)-(2.20) can be rewritten as follows

$$\boldsymbol{\varepsilon} = \mathbf{B}\boldsymbol{\delta} \tag{2.21}$$

where $\mathbf{B}$ is the strain matrix containing the derivatives of the shape functions, and $\boldsymbol{\delta}$ is the vector of the nodal displacements $\mathbf{u}_{ij}$ of the element. Denoting by $\boldsymbol{\sigma}$ the vector of the engineering component of the stress tensor, $\sigma = (\sigma_{xx}, \sigma_{yy}, \sigma_{zz}, \tau_{xy}, \tau_{xz}, \tau_{yz})^T$, within the element we have

$$\boldsymbol{\sigma} = \mathbf{D}\left(\boldsymbol{\varepsilon} - \boldsymbol{\varepsilon}_0\right) \tag{2.22}$$

where $\mathbf{D}$ is the matrix depending on the elastic constants E and v, and $\boldsymbol{\varepsilon}_0$ is the vector of the engineering components of the thermal dilatation $\alpha(T - T_0)\mathbf{I}$, with $\mathbf{I}$ the identity tensor and T_0 the reference temperature. As for calculation of the stiffness matrix, a four point Gauss-Legendre scheme is used for numerical integration in the (ξ, η) plane, while integration along the thickness is carried out analytically.

To define the geometry of the structure it is sufficient to input, for each layer, the coordinates of two non-adjacent vertices and the thickness h. Each layer of the pyramidal structure is modeled by one or more strata of elements (the number of strata must be specified by the user). The mesh of finite elements used for the thermo-mechanical analysis matches the grid of cells used by DJOSER. Regarding the boundary conditions applied to the whole structure, we assume that the base of the structure is clamped, thus precluding any displacements of the bottom surface of the lowest elements. Two superimposed elements are connected by assuming the top displacements of the lower element equal the bottom displacements of the upper element. This approach does not take into account the deformability of the adhesive layer, and any eventual debonding phenomena can be detected by means of an analysis of the shear and normal stresses.

3. Applications and results

The numerical tool described in Section 2 has been applied to the set of samples shown in Fig. 3, each composed of two square slabs with different dimensions: a semiconductor device substrate (12 mm wide and 0.6 mm thick) made of silicon (layer 2, Fig. 2(b)) and a lower heat dissipating frame (24 mm wide and 1 mm thick) made of copper (layer 1, Fig. 2(b)).

With the aim of illustrating the accuracy of the proposed numerical procedure, a comparison is presented with the results of standard finite element analyses using brick elements. The dependence of the numerical results on the number of elements in the grids is then investigated.

The two-dimensional heat sources, dissipating a total of 200 W, are localized on the top silicon surface. They are arranged in four square islands in the symmetric ("S") and asymmetric ("A") samples and in one central island in the "K" series (see Fig. 3). The samples belonging to the "K" group differ from each other in the 2-D cell densities used by both the thermal and mechanical solvers. The main properties of all samples are reported in Table I. The number of cells per side in the copper layer is twice that of the silicon one.

The two layers of all the samples are separated by a thermally resistive interface, representing a gluing or fixing film, whose specific contact thermal resistance R_c is 10 mm^2 °C/W. As for the thermo-mechanical properties, we have $E = 1.5\ 10^5$ N/mm^2, $v = 0.17$, and $\alpha = 8.0\ 10^{-6}$ °C^{-1} for the silicon, and $E = 1.130^5$ N/mm^2, $v = 0.34$, and $\alpha = 1.7\ 10^{-5}$ °C^{-1} for the copper.

Table I also includes a further sample, with the same characteristics as sample "S", on which an analysis has been conducted by removing the heat sources and considering the structure subjected
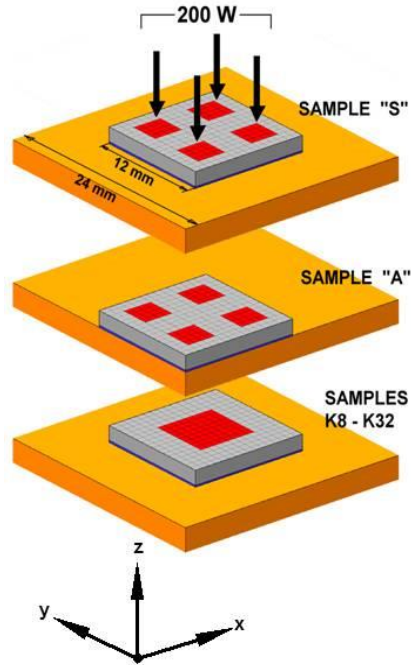
Fig. 3 Example applications

Table I

Sample	Thickness h_2 (Si)	Cells per side (Si)	Structure
S-UN	600 mm	32	symmetric
S	600 mm	32	symmetric
A	600 mm	32	asymmetric
K8	600 mm	8	symmetric
K16	600 mm	16	symmetric
K24	600 mm	24	symmetric
K32	600 mm	32	symmetric

to a uniform thermal variation $T - T_0 = 100$ ℃ (sample "S-UN").

The results of the thermo-mechanical analyses of the samples are shown and discussed below. The stress state at the interface between the substrate and copper layer and between the copper and silicon layer is described by the following quantities (Fig. 2)

$$P_{1x}^-(x, y) = \tau_{xz}(x, y, 0), \qquad P_{1y}^-(x, y) = \tau_{yz}(x, y, 0), \qquad Q_1^-(x, y) = \sigma_{zz}(x, y, 0),$$

$$P_{1x}^+(x, y) = \tau_{xz}(x, y, h_1), \qquad P_{1y}^+(x, y) = \tau_{yz}(x, y, h_1), \qquad Q_1^+(x, y) = \sigma_{zz}(x, y, h_1),$$

$$P_1^- = \sqrt{(P_{1x}^-)^2 + (P_{1y}^-)^2}, \qquad P_1^+ = \sqrt{(P_{1x}^+)^2 + (P_{1y}^+)^2}.$$

The numbers refer to the layer, and the sign indicates the top (+) and bottom (-) surfaces. We point out that, by virtue of the continuity of displacements at the interface between layers 1 and 2,
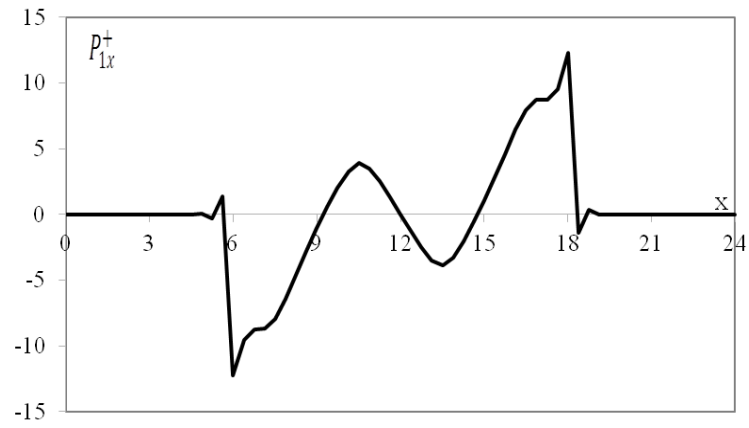
Fig. 4 Cross-section plot of shear stress P_{1x}^- (N/mm^2) vs. x (mm) for sample "S"

Fig. 5 Cross-section plot of normal stress Q_1^- (N/mm^2) vs. x (mm) for sample "S"

stresses P_{2x}^- , P_{2y}^- , Q_2^- coincide respectively with P_{1x}^+ , P_{1y}^+ and Q_1^+ moreover, P_{2x}^+ , P_{2y}^+ , Q_2^+ are zero because no loads are applied to the top of layer 2.

Fig. 4, Fig. 5, Fig. 6 and Fig. 7 shows the plots of the stresses P_{1x}^- , Q_1^- , P_{1x}^+ and Q_1^+ for sample "S" calculated in correspondence to the vertical cross-section intersecting the structure where the maximum temperature values occur.

The plots show that the most critical points for both normal and shear stresses are the edges of the upper layer, where the maximum values occur. In particular, the normal stress here has a strong compressive (negative) value, while the maximum tensile stress (positive), potentially dangerous for the integrity of the interface attachment, lies just beneath the center of the heat dissipating islands.

The global pattern of Q_1^- and P_1^- at the interface between the substrate and copper and of Q_1^+ and P_1^+ at the interface between copper and silicon is shown in Fig. 8 and Fig. 9.

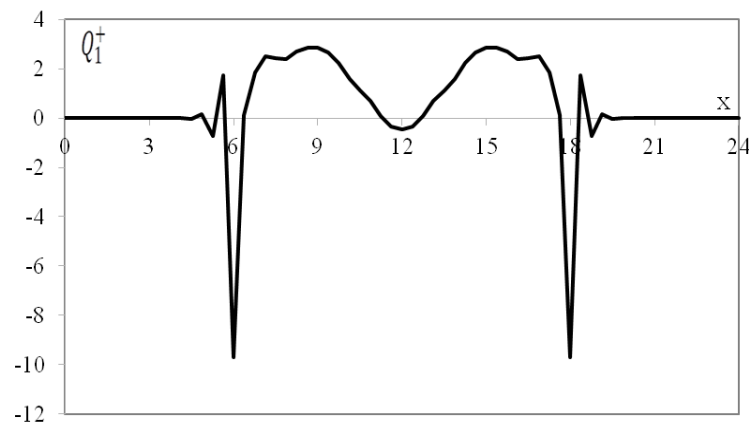Fig. 6 Cross-section plot of shear stress P_{1x}^+ (N/mm^2) vs. x (mm) for sample "S"

Fig. 7 Cross-section plot of normal stress Q_1^+ (N/mm^2) vs. x (mm) for sample "S"
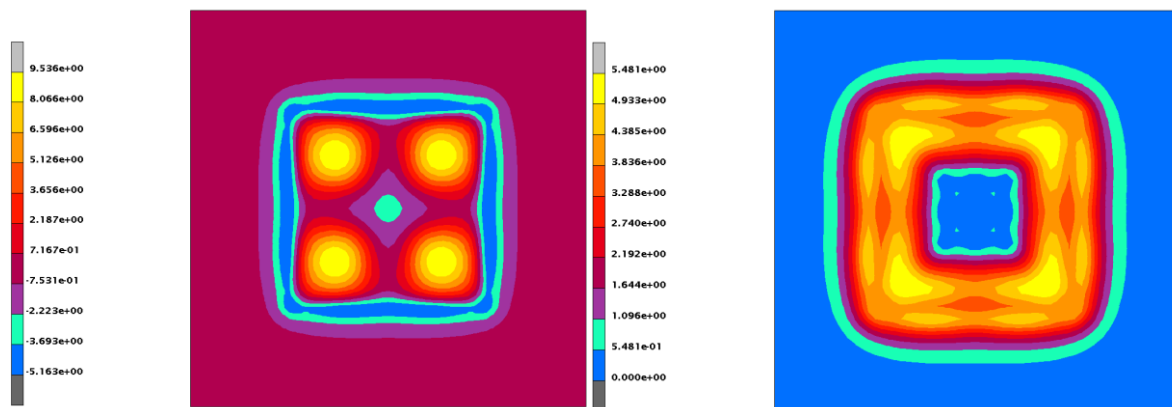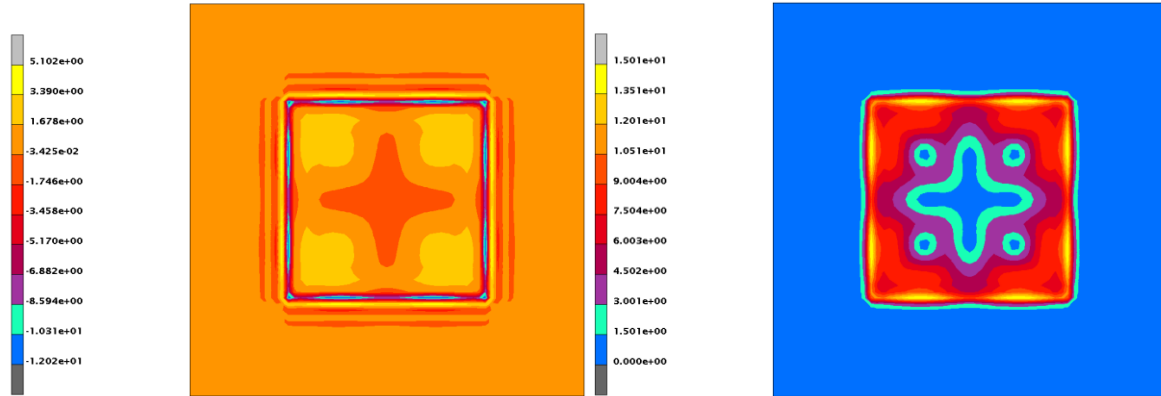

Fig. 8 Pattern of Q_1^- (left) and P_1^- (right)

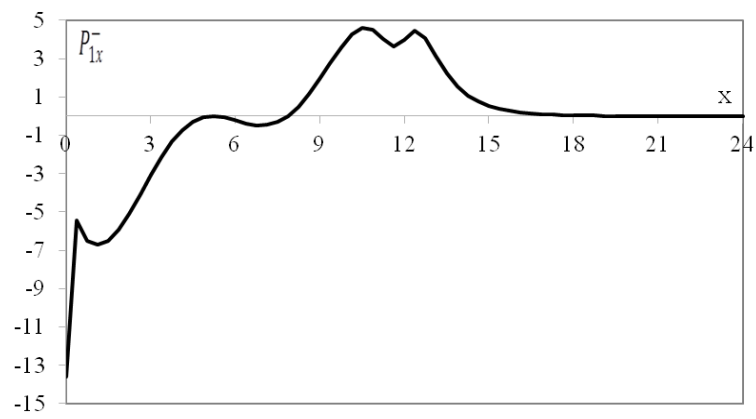Fig. 9 Pattern of Q_1^+ (left) and P_1^+ (right)

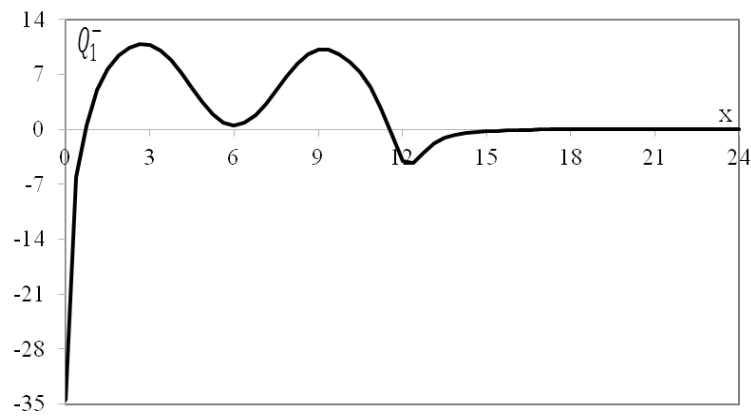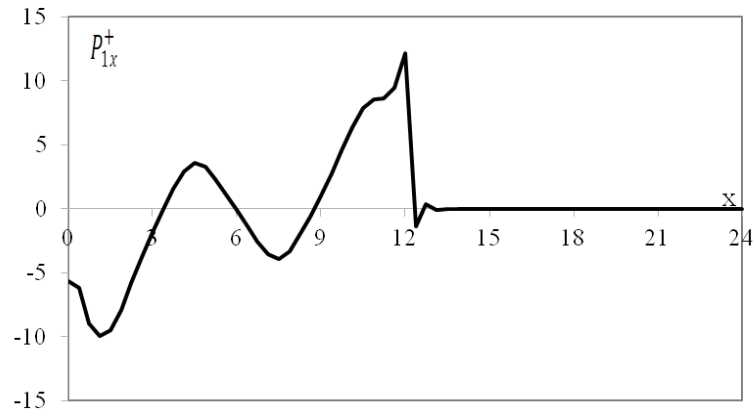Fig. 10 Cross-section plot of shear stress P_{1x}^- (N/mm^2) vs. x (mm) for sample "A"

Fig. 11 Cross-section plot of normal stress Q_1^- (N/mm^2) vs. x (mm) for sample "A"

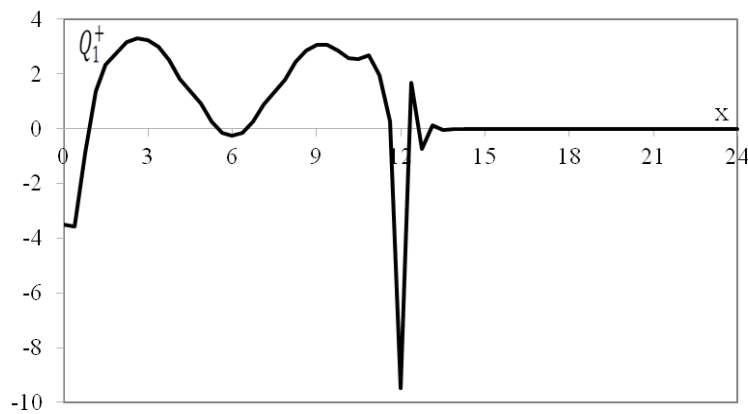Fig. 12 Cross-section plot of shear stress P_{1x}^{+} (N/mm^2) vs. x (mm) for sample "A"

Fig. 13 Cross-section plot of normal stress Q_{1}^{+} (N/mm^2) vs. x (mm) for sample "A"

Fig. 10, Fig. 11, Fig. 12 and Fig. 13 show the plots of the stresses P_{1x}^{-}, Q_{1}^{-}, P_{1x}^{+} and Q_{1}^{+} for sample "A" calculated in correspondence to the vertical cross-section intersecting the structure where the maximum temperature values occur.

Finally, by comparing the results for samples "S" and "A", the effect of the structural asymmetry is quite evident. In fact, in sample "A", the values of the normal and shear stresses reached at the copper-heat sink interface are greater than those in sample "S" (see P_{1x}^{-} and Q_{1}^{-} in Fig. 4 and Fig. 5). On the other hand, the values of the normal and shear stresses at the copper-silicon interface are similar in both "A" and "S", even if the maximum values are reached at different points.

The validation procedure is performed via thermo-mechanical analysis of the "K" series, and comparing the results with those obtained through standard finite element analysis by discretizing the structure with a very large number (30720) of 20-node brick elements. Fig. 14 shows the finite element mesh of the structure, the discretizion of the layers is 64×64×6 elements for the copper
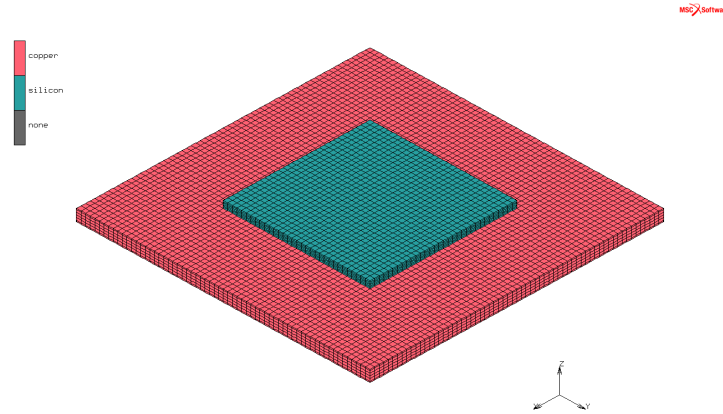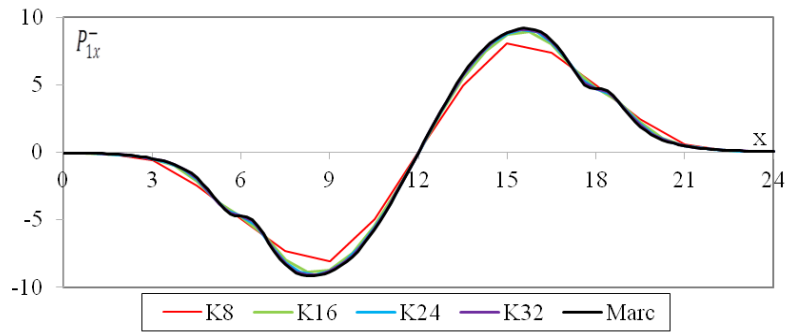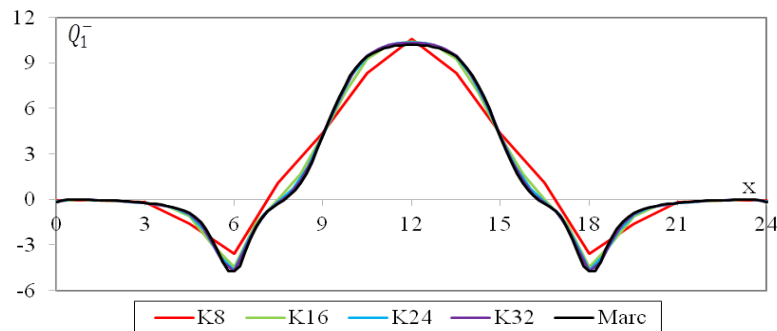
Fig. 14 Finite element mesh of the structure for the Marc analysis

Fig. 15 Cross-section plot of shear stress P_{1x}^- (N/mm^2) vs. x (mm) for samples K8-K32 (colored lines) as compared with the results from the Marc analysis (black lines)

Fig. 16 Cross-section plot of normal stress Q_1^- (N/mm^2) vs. x (mm) for samples K8-K32 (colored lines) as compared with the results from the Marc analysis (black lines)

and 32×32×6 for the silicon. The mesh is regular, except for the copper layer, in which the dimensions of the elements vary within the thickness.

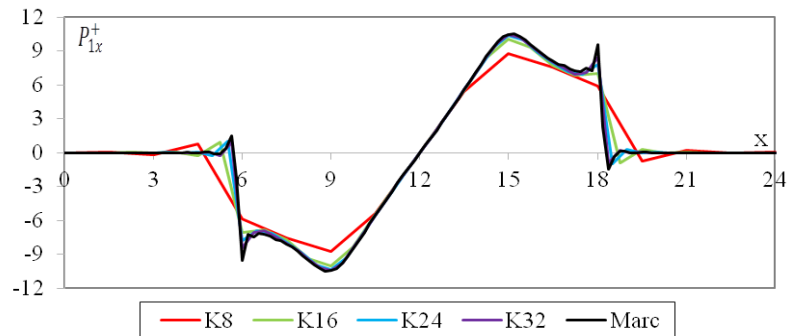The standard analysis has been conducted using the commercial code Marc (http://www.mscsoftware.com/).

Fig. 17 Cross-section plot of shear stress P_{1x}^+ (N/mm^2) vs. x (mm) for samples K8-K32 (colored lines) as compared with the results from the Marc analysis (black lines)
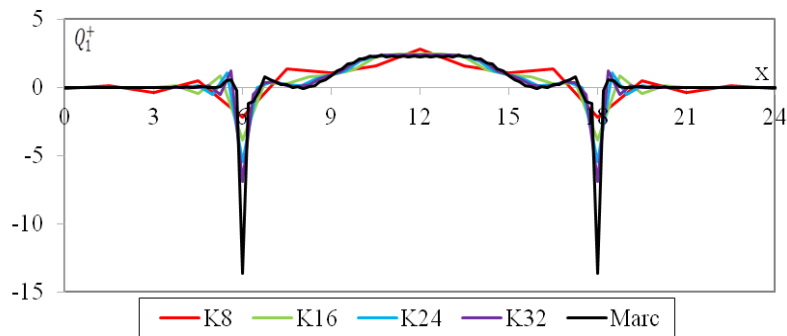

Fig. 18 Cross-section plot of normal stress Q_1^+ (N/mm^2) vs. x (mm) for samples K8-K32 (colored lines) as compared with the results from the Marc analysis (black lines)

Table II

SAMPLE	Cells per side (silicon)	Time (sec)
K8	8	23.3
K16	16	487.2
K24	24	2541.1
K32	32	8249.6
Marc		74185.9

The aim of the numerical tests is to investigate the dependence of the results on the cell density, and evaluate computation times. The results of these tests are presented in Fig. 15, Fig. 16, Fig. 17 and Fig. 18, which show the plots of stresses P_{1x}^-, Q_1^-, P_{1x}^+ and Q_1^+ corresponding to 8, 16, 24 and 32 cells per side (red, green, light blue and purple lines, respectively) and to the Marc finite element analysis (black line).

The figures show that the most critical points are the edges of the silicon layer, where the accuracy of the results depends heavily on the mesh refinement. On the other hand, the computation time required for the analysis increases with cell density, as reported in Table II, though it still remains well below the time needed for a Marc run with 30720 brick elements.

Finally, the results of the analysis performed on the "S-UN" sample is reported below. In this
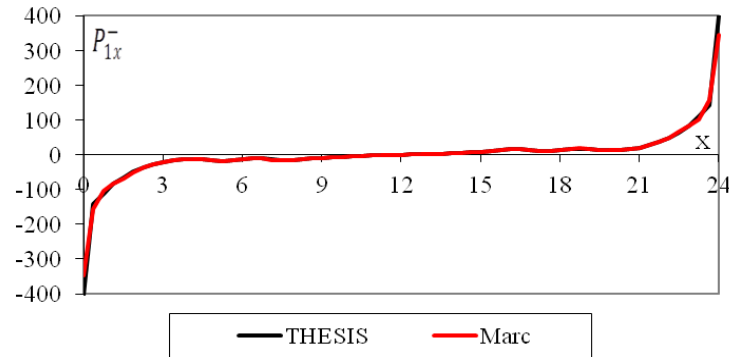
Fig. 19 Cross-section plot of shear stress P_{1x}^- (N/mm^2) vs. x (mm) for sample "S-UN" calculated via THESIS (black line) and Marc (red line)

Fig. 20 Cross-section plot of normal stress Q_1^- (N/mm^2) vs. x (mm) for sample "S-UN" calculated via THESIS (black line) and Marc (red line)

Fig. 21 Cross-section plot of shear stress P_{1x}^+ (N/mm^2) vs. x (mm) for sample "S-UN" calculated via THESIS (black line) and Marc (red line)
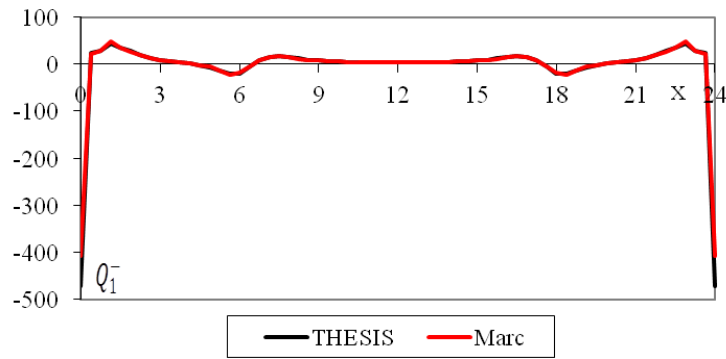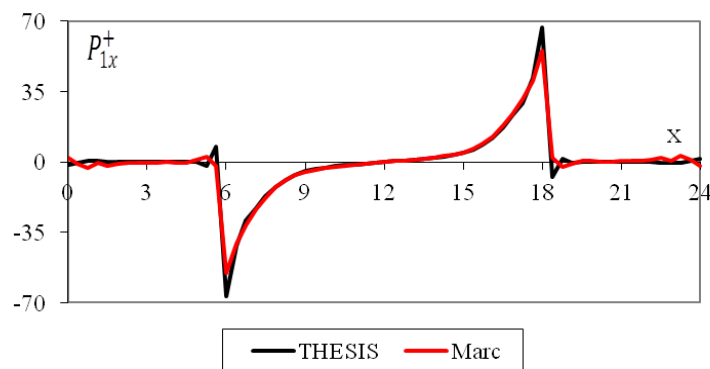
last sample the structure has been subjected to a uniform thermal variation of 100℃. Fig. 19, Fig. 20, Fig. 21 and Fig. 22 show the plots of the stresses P_{1x}^-, Q_1^-, P_{1x}^+ and Q_1^+ for sample "S-
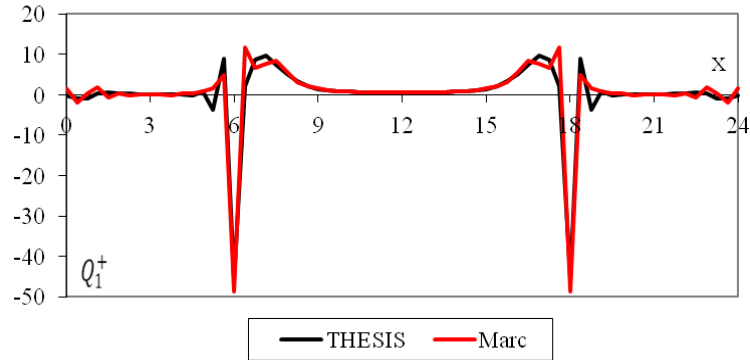
Fig. 22 Cross-section plot of normal stress Q_1^+ (N/mm^2) vs. x (mm) for sample "S-UN" calculated via THESIS (black line) and Marc (red line)

UN", calculated in the middle cross-section, vs. x. As can be seen, once again in this case, the stresses reach high values, especially at the boundaries of both the layers and the results of the Marc analysis substantially match those obtained with THESIS.

4. Conclusions

In this paper a numerical mathematical tool for the thermo-mechanical analysis of power electronic devices and their assemblies has been presented. The aim of the tool is simply to equip the recently proposed, user-friendly, analytical thermal simulator DJOSER with a suitable mechanical solver, called THESIS, so that the resulting temperature maps may also be used to calculate the thermally induced mechanical stresses and strains. The advantages of this simulation strategy concern both calculation times and the possibility of using uniform rectangular meshes within the body layers based on the 2-D meshes used by DJOSER for the temperature mapping. Due to the extreme complexity of a fully analytical solution to the mechanical problem, the mechanical solver was developed following a finite element strategy, though making use of a new, expressly developed THESIS element, as described in detail in Subsection 2.2.

The validation tests performed on the samples illustrated in Fig. 3 were carried out by comparing the THESIS results with those obtained via standard finite element analysis performed with the commercial code Marc and twenty-nodes brick elements. As expected, this comparison clearly shows that the accuracy of results depends on the cell density, with the error being highest near the borders, where the Marc code also presents singularity points and consequently undergoes a fall in accuracy. Thus, in order to obtain accurate results on the whole structure, it is recommended that the number of cells utilized not be less than a certain limit, also in light of the fact that THESIS computational times nevertheless remain considerably lower than Marc ones.

Therefore, thanks to its user-friendliness and the ease of model building, which provides a high degree of automatization, the coupled DJOSER-THESIS simulation system for thermo-mechanical analyses of packaged power electronic devices may be a suitable substitute for the more expensive numerical tools currently in use in small- and medium-sized enterprises involved in electronic device manufacturing.

References

Bagnoli, P.E., Bartoli, C. and Stefani, F. (2007a), "Validation of the DJOSER Analytical thermal simulator for electronic power devices and assembling structures", *Microelectron. J.*, **38**, 185-196.

Bagnoli, P.E, Casarosa, C. and Stefani, F. (2007b), "DJOSER: analytical thermal simulator for multilayer electronic structures. theory and numerical implementation", *Proceedings of Thermal Issues in Emerging Technologies Conference, ThETA 1*, Cairo, January.

Bagnoli, P.E., Padovani, C., Pagni, A. and Pasquinelli, G. (2008), "Integrating a thermo-mechanical solver into the DJOSER analytical thermal simulator for multilayer power electronic assemblies. Preliminary results", *Proceedings of the Second International Conference on Thermal Issues in Emerging Technologies*, Cairo, December.

Bagnoli, P.E., Girardi, M., Padovani, C., Pagni, A. and Pasquinelli, G.. (2009), "Thermo-mechanical solver for multi layer packages of power electronic devices and systems. Preliminary results", *Proceedings of the UIT 2009 - 27th UIT National Heat Transfer Conference*, Reggio Emilia, June.

Bagnoli, P.E., Girardi, M., Padovani, C., Pagni, A. and Pasquinelli, G. (2010), "Thermo-mechanical analysis of 3-d multilayer structures for power electronic devices", *THETA3 - Proceedings of the Third International Conference on Thermal Issues in Emerging Technologies - Theory and Applications*, Cairo, December.

Bagnoli, P.E., Padovani, C., Pagni, A. and Pasquinelli, G. (2011), "A thermo-mechanical solver for multilayer power electronic assemblies integrated into the DJOSER thermal simulator", *J. Electr. Packag.*, **133**, 011005-1 - 011005-7.

Carrera, E. (2004), "On the use of the Murakami's zig-zag function in the modeling of layered plates and shells", *Comput. Struct.*, **82**, 541-554.

Crosby, T. and Ghoniem, N.M. (2011) "Thermo-Mechanical damage of tungsten surfaces exposed to rapid transient plasma heat loads", *Interact. Multiscale Mech.*, **4** (3), 207-217.

De Borst, R. and Sadowski, T. (2008). *Lecture notes in composite materials - Current topics and achievements,* Springer.

Gherlone, M. and Di Sciuva, M. (2007), "Thermo-mechanics of undamaged and damaged multilayered composite plates: assessment of the FEM sub-laminates approach", *Compos. Struct.*, **81**, 137-155.

Grigolyuk, E.I. and Tolkachev, V.M. (1980), *Contact problems in the theory of plates and shells,* Mir Publishers, Moscow.

Grigolyuk, E.I., Kogan, Y.A. and Mamai, V.I. (1994), "Problems of the deformation of thin-walled laminated structures with layer separation", *Ross. Akad. Nauk MTT*, **2**, 6-32.

Grigolyuk, E.I., Kogan, Y.A. and Mamai, V.I. (1995), "A model of the deformation of a non-uniformly heated three-layers rod with delaminations", *J. Appl. Math. Mech.*, **59** (3), 449-457.

Hsueh, C.H., Lee, S.B. and Lin, H.Y. (2006), "Analyses of mode I edge delamination by thermal stresses in multilayer systems", *Compos., Part B*, **37**, 1-9.

Lo, S.H., Zhen, W., Sze, K.Y. and Chen, W.J. (2011), "C0-type global–local theory with non-zero normal strain for the analysis of thick multilayer composite plates", *Comput. Mech.*, **47**, 479-491.

Montesi, M., Bagnoli, P.E., Casarosa, C. and Pasquinelli, G. (2004), "Steady-state thermal mapping of electronic devices with multi-layer stack mountings by analytical relationships", *Proceedings of ITSS II ASME–ZSIS Conference*, Bled, Slovenia, June.

Robaldo, A. (2006), "Finite element analysis of the influence of temperature profile on thermoelasticity of multilayered plates", *Comput. Struct.*, **84**, 1236-1246.

Saidi, H., Houari, M.S.A., Tounsi, A. and Adda Bedia, E.A. (2013), "Thermo-mechancal bending response with stretching effect of functionally graded sandwich plates using a novel shear deformation theory", *Steel Compos. Struct.*, **15**, 221-245.

Simhonian, A.M. and Sanoyan, Y.G. (2009), "Investigation of the plane stress state of a multilayer structure under heat variations", *Mech. Solid.*, **44**(5), 756-761.

Suhir, E. and Weld, J.D. (1998), "Application of a 'surrogate' layer for lower bending stress in a vulnerable

material of a tri-material body", *Microelectron. Reliab.*, **38**, 1949-1954.

Suhir, E. (2000), "Adhesively bonded assemblies with identical nondeformable adherends and 'piecewise continuous' adhesive layer: predicted thermal stresses in the adhesive", *Int. J. Solid. Struct.*, **37**, 2229-2252.

Suhir, E. (2011), "Predictes stresses in die-carrier assemblies in "stretchable" electronics: is there an incentive for using a compliant bond", *ZAMM Z. Angew. Math. Mech.*, **91**(1), 57-67.

Timoshenko, S.P. and Woinowsky-Krieger, S. (1959), *Theory of plates and shells*, McGraw-Hill Internatioal Editions.

Wu, L.Z. (2004), "Thermoelastic analysis of chip-substrate system", *J. Electron. Packag.*, **126**, 326-332.

Xie, W.D. and Sitaraman, S.K. (2000), "Interfacial thermal stress analysis of anisotropic multi-layered eletronic packaging structures", *J. Electron. Packag.*, **122**, 66-68.

Zhen, W. and Chen, W.J. (2007), "A quadrilateral element based on refined global-local higher-order theory for coupling bending and extension thermo-elastic multilayered plates", *Int. J. Solid. Struct.*, **44**, 3187-3217.

Zienkiewicz, O.C. and Taylor, R.L. (1989), *The Finite Element Method, Basic formulation and linear problems*, Fourth Edition, Volume 1, McGraw-Hill, London, UK.